IET Generation, Transmission & Distribution

Special Issue: New Trends in Wide-Area Monitoring and Control of Power Systems with Large Scale Renewables

Novel pair-wise relative energy function for transient stability analysis and real-time emergency control

ISSN 1751-8687
Received on 19th October 2016
Revised 10th March 2017
Accepted on 9th April 2017
E-First on 21st August 2017
doi: 10.1049/iet-gtd.2016.1671
www.ietdl.org

Jing Gou[1], Youbo Liu[2] ✉, Junyong Liu[2], Gareth A. Taylor[3], Mohsen M. Alamuti[4]

[1]*State Grid Sichuan Power Economic Research Institute, 366 West Shuxiu Road, High-Tech District, Chengdu 610041, People's Republic of China*

[2]*School of Electrical Engineering and Information, Sichuan University, 24 First Ring Road, Wuhou District, Chengdu 610065, People's Republic of China*

[3]*Department of Electronic and Computer Engineering, Brunel University London, Kingston Lane, Uxbridge Middlesex UB8 3PH, United Kingdom*

[4]*GB System Capability Assessment, National Grid, Warwick CV34 6DA, UK*

✉ *E-mail: liuyoubo@scu.edu.cn*

Abstract: In recent years, situation awareness and risk mitigation have become the challenging issues in large-scale power grids. This study presents a novel pair-wise relative energy function for real-time transient stability analysis and emergency control. The proposed energy function is able to accurately identify the clusters of critical and non-critical generators significantly faster when compared with previous methods. Additionally, a new emergency control criterion is proposed in order to stabilise the identified critical generators within a comparatively short interval after fault clearance. The emergency control scheme computes the capacity of the requisite generation curtailment using the pre-calculated relative energy of the equivalent post-fault system. Finally, the relative energy oscillation trajectories that occur in the critical cluster are utilised in order to locate the most appropriate generator to launch the emergency control. When compared with the existing methods, it is evident that the novel approach can be applied practically for power systems transient stability analysis and emergency control. The effectiveness of the proposed method is demonstrated and evaluated using the New England 10 machines 39-bus and 16 machines 68-bus systems.

1 Introduction

Modernisation of power systems is increasing the penetration of renewable power generation resources, as well as deployment of monitoring and measurement infrastructures [1]. Although such developments create efficient and environmentally friendly energy infrastructures, the subsequent stochastic behaviour in generation, transmission and distribution systems has further complicated power system transient stability problems. Disastrous power blackouts [2, 3] alert the system operators that serious consequences, such as out-of-step separation and cascading failures, might occur easily without having an accurate, rapid and real-time stability analysis and emergency control infrastructure in place. Implementation of such systems offers a second line of defence against such wide spread blackouts.

The majority of transient stability analysis techniques perform a set of studies on the simulated network model to assess the stability properties of the power system. However, in some cases, particularly during fault conditions, detailed knowledge of the network may not be fully available. As a result, network parameters have to be estimated through a subsequent post-processing method to validate the approximate network model [4]. In order to overcome this limitation, a hybrid stability analysis technique known as single machine equivalents (SIME) [5, 6], seeks to circumvent this limitation by using a hybrid methodology for transient stability analysis. This is suitable for offline analysis, but may not be adequate for real-time security assessment. In parallel, a number of studies have also demonstrated that the energy function-based technique is one of the most promising techniques with regard to revealing the dynamic nature of power system transient stability [7–10].

The increasing application of wide area measurement systems (WAMS) has altered the research focus from *offline decision, real-time matching* schemes [11] to *online decision, real-time control* strategies [12–14]. Consequently, it is widely acknowledged that accurate identification of critical machines cluster (CMC), fast assessment of emergency control criterion, reliable calculation of control curtailment and appropriate selection of control location are the determining performance factors with regard to the execution of real-time stability analytics and emergency control strategies. Therefore, a method is required that enables real-time monitoring of transient stability utilising specific data that is available from phasor measurement unit (PMU) measurements.

To address the above requirements, a novel pair-wise relative energy function is proposed in this paper, providing a new scheme of fast and real-time transient stability analysis and emergency control. The proposed method is independent of the detailed power system model. Only PMU data from the monitored generator nodes is required to perform the stability analysis and emergency control simulations. The paper proceeds in Sections 2 and 3 by providing a derivation that justifies the use of the novel pair-wise generators relative energy measures as an estimate of post-fault system transient energy. Subsequently, the real-time measurements are further utilised to extract generator separation patterns, compute emergency generation curtailment and select the control location in Section 4. The method is tested on a variety of fault simulations. The presented simulation results demonstrate the practical application with regard to power systems transient stability analysis and emergency control.

2 Relative energy of pair-wise generators

2.1 Relative kinetic energy

In a multi-machine power system containing G_i, G_j, …, G_N generators, the mechanical power input and electromagnetic power output of each generator can be expressed as $P_{\mathrm{m}i}$, $P_{\mathrm{m}j}$, …, $P_{\mathrm{m}N}$ and P_{ei}, P_{ej}, …, P_{eN}, respectively. Choosing any two generators from the system can create a pair-wise generator set shown in Fig. 1.

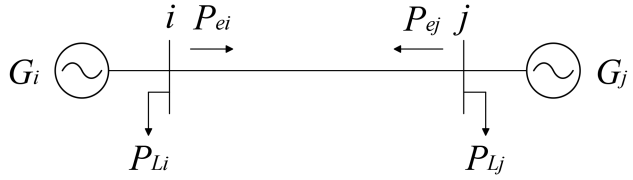

Fig. 1 *Pair-wise generators description of multi-machine power systems*

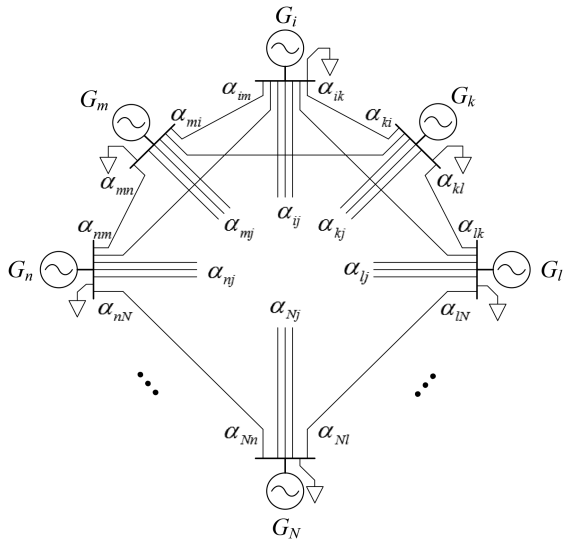

Fig. 2 *Reduced-order network containing only dynamic generator nodes*

Taking pair-wise generators G_i–G_j as an example, the rotor swing equations in the synchronous coordinate system can be written as

$$\begin{cases} M_{ij}\dfrac{\mathrm{d}\omega_{ij}}{\mathrm{d}t} = P_{\mathrm{m}ij} - P_{\mathrm{e}ij} \\ \dfrac{\mathrm{d}\delta_{ij}}{\mathrm{d}t} = \omega_{ij} \end{cases} \tag{1}$$

where ω_{ij} denotes the relative rotor speed, δ_{ij} denotes the relative rotor angle, $M_{ij} = M_iM_j/(M_i + M_j)$ is the equivalent inertial coefficient and $P_{\mathrm{m}ij}$, $P_{\mathrm{e}ij}$ can be described as $P_{\mathrm{m}ij} = M_jP_{\mathrm{m}i}/(M_i + M_j) - M_iP_{\mathrm{m}j}/(M_i + M_j)$, $P_{\mathrm{e}ij} = M_jP_{\mathrm{e}i}/(M_i + M_j) - M_iP_{\mathrm{e}j}/(M_i + M_j)$. Equation (1) is similar to the rotor swing equation of the one machine infinity bus (OMIB) system. The single rotor kinetic energy as defined in the transient energy function (TEF) is based on the rotor swing equation of the OMIB. Taking this concept, we define the relative kinetic energy of pair-wise generators G_i–G_j using the following expression:

$$V_{\mathrm{K}ij} = \frac{1}{2}M_{ij}\omega_{ij}^2 \tag{2}$$

Expanding the above general expression to the arbitrary pair-wise generators of a N-machine system, the relative kinetic energy set (RKES) of the system can be defined as

$$\mathrm{RKES} = \left\{K_{REi-j} \middle| i, j \in G, j \neq i\right\} \tag{3}$$

Generalisation of this definition yields an expression in the form of

$$K_{REi-j} = f(M_i, M_j, \omega_{ij} | i, j \in G) = \frac{1}{2}M_{ij}\omega_{ij}^2 \tag{4}$$

2.2 Relative potential energy

The relative potential energy (per unit value based on potential energy at time t_0) across a given line segment after a disturbance is defined as

$$V_{\mathrm{P}_{ij}} = \int_{\theta_{ij,0}}^{\theta_{ij}} [P_{ij}(u) - P_{ij,s}]\,\mathrm{d}u = \int_{t_0}^{t} \Delta P_{ij}\omega_{ij}\,\mathrm{d}t \tag{5}$$

where ΔP_{ij} is the per unit value of the net power flow through the line l_{ij} and ω_{ij} is the frequency difference between the both ends of a line.

Referring to the simplified network diagram of Fig. 2, a multi-machine power grid can be equivalently represented as a network that only contains the dynamic generator nodes. Accordingly, the power flow along a generator-connected line is a proportion of the net power flow from the internal generator bus. This proportion is determined by the steady-state generator set points and the network parameters, which are encapsulated in the coefficients α. Naturally, according to conservation of energy, the sum of the α coefficients pertaining to a single generator node must be unity

$$\sum\nolimits_{j=1, j\neq i}^{N} \alpha_{ij} = 1 \tag{6}$$

Utilising this definition, the total system post-fault potential energy is found to be

$$\begin{aligned} V_{\mathrm{P}} &= \sum_{L} V_{\mathrm{P}_{ij}} = \sum_{i=1}^{N-1}\sum_{j=i+1}^{N}\int_{t_0}^{t} \alpha_{ij}\Delta P_{Gi}\omega_{ij}\,\mathrm{d}t \\ &= \frac{1}{2}\sum_{i=1}^{N}\sum_{j=1, j\neq i}^{N}\int_{t_0}^{t} \alpha_{ij}\Delta P_{Gi}\omega_{ij}\,\mathrm{d}t \end{aligned} \tag{7}$$

where L is the set of lines in the system, and V_{P} is the total relative potential energy.

Considering the principle of superposition with regard to the frequency $\omega_{ij} = \omega_i - \omega_j = \omega_{ik} + \omega_{kj}$ as well as the consistency of power flow direction through a line $\alpha_{ij}\Delta P_{Gi} = \alpha_{ji}\Delta P_{Gj}$, the total relative potential energy is derived as

$$\begin{aligned} V_{\mathrm{P}} &= \frac{1}{2}\sum_{i=1}^{N}\sum_{j=1, j\neq i}^{N}\int_{t_0}^{t} (\alpha_{ij}\Delta P_{Gi}\omega_{ik} + \alpha_{ji}\Delta P_{Gj}\omega_{jk})\,\mathrm{d}t \\ &= \sum_{i=1}^{N}\int_{t_0}^{t} \Delta P_{Gi}\omega_{ik}\,\mathrm{d}t \end{aligned} \tag{8}$$

where the index k specifies any generator in the system the same as generators i and j.

The obtained equation for total potential energy (V_{P}) eliminates all dependence on the coefficients α. Consequently, the total potential energy in the system can be written in terms of the generator properties alone. Subsequently, information obtained from generators is used to define a relative potential energy set (RPES) index in order to evaluate total potential energy for the whole system

$$\mathrm{RPES} = \left\{P_{REi-j} \middle| i, j \in G, j \neq i\right\} \tag{9}$$

The extension of RPES index yields [15]

$$\begin{aligned} P_{REi-j} &= g(\Delta P_i, \Delta P_j, \omega_{ij} | i, j \in G) \\ &= \int_{t_0}^{t} \frac{1}{N}[\Delta P_{Gi}(t) - \Delta P_{Gj}(t)]\omega_{ij}\,\mathrm{d}t \end{aligned} \tag{10}$$

Using hypothetical coefficient β to replace $1/N$ in the above equation, the total potential energy yielded from the pair-wise components can be rewritten as

$$\begin{aligned} V_{\mathrm{RPE}} &= \sum_{i=1}^{N-1}\sum_{j=i+1}^{N}\int_{t_0}^{t} \frac{1}{N}[\Delta P_{Gi}(t) - \Delta P_{Gj}(t)]\omega_{ij}\,\mathrm{d}t \\ &= \frac{1}{2}\sum_{i=1}^{N}\sum_{j=1, j\neq i}^{N}\int_{t_0}^{t} \beta\Delta P_{Gij}\omega_{ij}\,\mathrm{d}t \end{aligned} \tag{11}$$

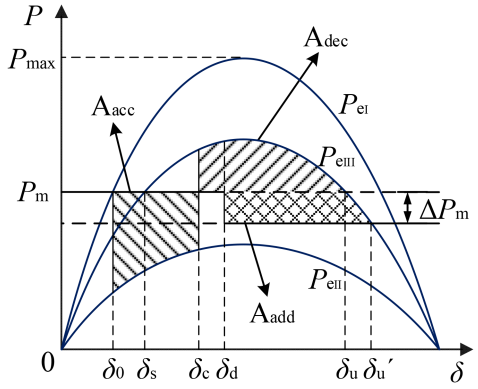

Fig. 3 *Power–angle of the equivalent power system*

The output volatility of each generator can be formulated as a function of the generated power variation of all other generators connected to the system. Taking this fact into account along with expanding the integral term in (11), the total post-fault potential energy can be derived as

$$\begin{aligned} V_{\mathrm{RPE}} &= \frac{1}{2}\sum_{i=1}^{N}\sum_{j=1,j\neq i}^{N}\int_{t_0}^{t}(\beta\Delta P_{Gij}\omega_{ik}+\beta\Delta P_{Gji}\omega_{jk})\,\mathrm{d}t \\ &= \sum_{i=1}^{N}\int_{t_0}^{t}N\beta\Delta P_{Gi}\omega_{ik}\,\mathrm{d}t=\sum_{i=1}^{N}\int_{t_0}^{t}\Delta P_{Gi}\omega_{ik}\,\mathrm{d}t=V_{\mathrm{P}} \end{aligned} \tag{12}$$

The above equation describing total post-fault potential energy reveals that the total potential energy can be written merely in terms of pair-wise generators power interactions.

The pair-wise relative energy is a virtual energy which is composed of the relative kinetic and potential energy. The former is mainly due to the relative rotor motion of pair-wise generators and the latter represents the relative oscillation status of pair-wise generators in the post-fault state. Consequently, the relative energy shows the electrical interaction between pair-wise generators compared with the TEF of the simplified equivalent system.

3 Energy features of post-fault power systems

3.1 Energy features of fault clearing point

Due to the energy conservation between injected mechanical kinetic energy and network electromagnetic energy, the status of transient stability is a reflection of the unbalanced energy absorption within the power network. Therefore, analysis of transient energy flow is critical for determining stability, which is primarily represented by the exchange between kinetic and potential energy. The referenced literature [16] shows that desynchronisation normally appears between the CMC and the non-CMC (NMC) after a severe disturbance or fault. The relative energy between the two generators in the identical cluster makes little contribution to the system instability. That is to say, the loss of stability mainly stems from the relative energy between specific generators that exist in the different clusters.

In a multi-machine power system, the CMC_S and NMC_A can be defined as

$$\begin{cases} \delta_S=(\sum_{i\in S}M_i\delta_i)/M_S & (M_S=\sum_{i\in S}M_i) \\ \delta_A=(\sum_{j\in A}M_j\delta_j)/M_A & (M_A=\sum_{j\in A}M_j) \end{cases} \tag{13}$$

When a multi-machine system is equivalently simplified in form of SIME, the rotor swing equation yields

$$\begin{cases} \delta=\delta_S-\delta_A \\ M_{\mathrm{eq}}=M_SM_A/(M_S+M_A) \\ \mathrm{d}^2\delta/\mathrm{d}t^2=M_{\mathrm{eq}}^{-1}(P_{\mathrm{m}}-P_{\mathrm{e}}) \end{cases} \tag{14}$$

where $P_{\mathrm{m}}=(M_S+M_A)^{-1}(M_A\sum_{i\in S}P_{\mathrm{m}i}-M_S\sum_{j\in A}P_{\mathrm{m}j})$ and $P_{\mathrm{e}}=(M_S+M_A)^{-1}(M_A\sum_{i\in S}P_{\mathrm{e}i}-M_S\sum_{j\in A}P_{\mathrm{e}j})$.

According to the corrected TEF (CTEF) [17, 18], energy is conserved after the fault clearance, as described by the following equation:

$$V=V_{\mathrm{K}}^{\mathrm{co}}+V_{\mathrm{P}}^{\mathrm{co}}=\frac{1}{2}M_{\mathrm{eq}}\omega^2+\int_{\delta_{\mathrm{s}}}^{\delta}-(P_{\mathrm{m}}-P_{\mathrm{e}})\,\mathrm{d}\delta=\mathrm{const} \tag{15}$$

Hence, the relative energy of post-fault power systems in terms of the unbalance power flows in (15) can be defined as

$$E_{RE}(\delta)=\int_{\delta_0}^{\delta}(P_{\mathrm{m}}-P_{\mathrm{e}})\,\mathrm{d}\delta \tag{16}$$

where δ_0 is the pre-fault stable state angle.

Referring to the power–angle curve of the equivalent system in Fig. 3, in which δ_{s}, δ_{c}, δ_{d}, δ_{u}, δ_{u}' represent the angles at the post-fault stable equilibrium point, fault clearing point, control implementation point, post-fault unstable equilibrium point (UEP) and post-control UEP, respectively, the relative energy at fault clearing point is found to be

$$\begin{aligned} E_{RE}(\delta_{\mathrm{c}})&=A_{\mathrm{acc}}=\int_{\delta_0}^{\delta_{\mathrm{c}}}(P_{\mathrm{m}}-P_{\mathrm{eII}})\,\mathrm{d}\delta=\int_{\delta_0}^{\delta_{\mathrm{c}}}\left(M_{\mathrm{eq}}\frac{\mathrm{d}\omega}{\mathrm{d}t}\right)\mathrm{d}\delta \\ &=\frac{1}{2}M_{\mathrm{eq}}\omega^2\Big|_{\omega_0}^{\omega_{\mathrm{c}}}=\frac{1}{2}M_{\mathrm{eq}}\omega_{\mathrm{c}}^2 \end{aligned} \tag{17}$$

The above equation demonstrates the equivalence between the relative energy and the corrected transient kinetic energy at the fault clearing point, which also corresponds to the acceleration area in the equal area criterion (EAC).

3.2 Energy features of emergency control point

Referring to the EAC method, the relative deceleration energy corresponding to the deceleration area can be defined as

$$\begin{aligned} A_{\mathrm{dec}}&=\int_{\delta_{\mathrm{c}}}^{\delta_{\mathrm{u}}}-(P_{\mathrm{m}}-P_{\mathrm{eIII}})\,\mathrm{d}\delta=\int_{\delta_{\mathrm{c}}}^{\delta_{\mathrm{d}}}(P_{\mathrm{eIII}}-P_{\mathrm{m}})\,\mathrm{d}\delta \\ &+\int_{\delta_{\mathrm{d}}}^{\delta_{\mathrm{u}}}(P_{\mathrm{eIII}}-P_{\mathrm{m}})\,\mathrm{d}\delta \end{aligned} \tag{18}$$

If $A_{\mathrm{dec}}<A_{\mathrm{acc}}$, the system will be unstable in the post-fault duration. Therefore, an emergency control in the form of generation curtailment ΔP_{m} is implemented, which aims to resynchronise the power system. Substituting into the above formula, the increased relative deceleration energy is

$$A_{\mathrm{add}}=\int_{\delta_{\mathrm{d}}}^{\delta_{\mathrm{u}}'}-(P_{\mathrm{m}}-\Delta P_{\mathrm{m}}-P_{\mathrm{eIII}})\,\mathrm{d}\delta\approx\frac{1}{2}(\delta_{\mathrm{u}}-\delta_{\mathrm{d}}+\delta_{\mathrm{u}}'-\delta_{\mathrm{d}})\Delta P_{\mathrm{m}} \tag{19}$$

In order for the system to remain stable, the following equation holds:

$$A_{\mathrm{acc}}=A_{\mathrm{dec}}+A_{\mathrm{add}} \tag{20}$$

Substituting (17)–(19) into (20) yields

$$\begin{aligned} \frac{1}{2}M_{\mathrm{eq}}\omega_{\mathrm{c}}^2&=\int_{\delta_{\mathrm{c}}}^{\delta_{\mathrm{d}}}(P_{\mathrm{eIII}}-P_{\mathrm{m}})\,\mathrm{d}\delta+\int_{\delta_{\mathrm{d}}}^{\delta_{\mathrm{u}}}(P_{\mathrm{eIII}}-P_{\mathrm{m}})\,\mathrm{d}\delta \\ &+\frac{1}{2}(\delta_{\mathrm{u}}+\delta_{\mathrm{u}}'-2\delta_{\mathrm{d}})\Delta P_{\mathrm{m}} \end{aligned} \tag{21}$$

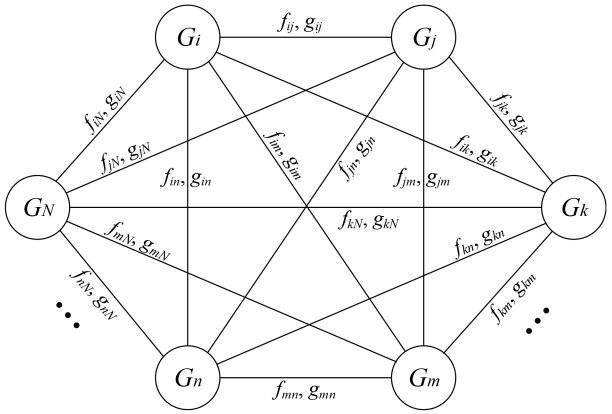

Fig. 4 *Undirected edge weighted graph of N generators system*

According to the CTEF, the energy of the equivalent system must remain constant at the both fault clearing and control implementation points, which is shown by

$$\begin{aligned}&\frac{1}{2}M_{\mathrm{eq}}\omega_{\mathrm{c}}^2+\int_{\delta_{\mathrm{s}}}^{\delta_{\mathrm{c}}}-(P_{\mathrm{m}}-P_{\mathrm{eIII}})\,\mathrm{d}\delta\\&=\frac{1}{2}M_{\mathrm{eq}}\omega_{\mathrm{d}}^2+\int_{\delta_{\mathrm{s}}}^{\delta_{\mathrm{d}}}-(P_{\mathrm{m}}-P_{\mathrm{eIII}})\,\mathrm{d}\delta\end{aligned}\tag{22}$$

Thus, simplifying the above expression yields

$$\int_{\delta_{\mathrm{c}}}^{\delta_{\mathrm{d}}}(P_{\mathrm{eIII}}-P_{\mathrm{m}})\,\mathrm{d}\delta=\frac{1}{2}M_{\mathrm{eq}}\omega_{\mathrm{c}}^2-\frac{1}{2}M_{\mathrm{eq}}\omega_{\mathrm{d}}^2\tag{23}$$

which can be rewritten as

$$E_{\mathrm{RE}}(\delta_{\mathrm{d}})=\frac{1}{2}M_{\mathrm{eq}}\omega_{\mathrm{c}}^2+\int_{\delta_{\mathrm{c}}}^{\delta_{\mathrm{d}}}(P_{\mathrm{eIII}}-P_{\mathrm{m}})\,\mathrm{d}\delta=\frac{1}{2}M_{\mathrm{eq}}\omega_{\mathrm{d}}^2\tag{24}$$

The obtained derivation of (24) proves that the relative energy is equal to the corrected transient kinetic energy at the control implementation point. Substituting (24) back into (21) yields

$$\begin{aligned}&E_{\mathrm{RE}}(\delta_{\mathrm{d}})=\frac{1}{2}M_{\mathrm{eq}}\omega_{\mathrm{d}}^2=\int_{\delta_{\mathrm{d}}}^{\delta_{\mathrm{u}}}(P_{\mathrm{eIII}}-P_{\mathrm{m}})\,\mathrm{d}\delta\\&+\frac{1}{2}(\delta_{\mathrm{u}}+\delta_{\mathrm{u}}'-2\delta_{\mathrm{d}})\Delta P_{\mathrm{m}}\end{aligned}\tag{25}$$

which shows that the corrected transient kinetic energy at the control implementation point is the sum of the remaining relative deceleration energy and the increased relative deceleration energy.

3.3 Relation of relative energy and EAC

According to the EAC, the acceleration area and deceleration area are normally used to estimate the stability margin. At the critical stable point, these two areas should be equal

$$\int_{\delta_0}^{\delta_{cr}}(P_{\mathrm{m}}-P_{\mathrm{e}})\,\mathrm{d}\delta=\int_{\delta_{\mathrm{cr}}}^{\delta_u}(P_{\mathrm{e}}-P_{\mathrm{m}})\,\mathrm{d}\delta\tag{26}$$

where δ_{cr} is the critical stable state angle. Equation (26) can also be represented as

$$\int_{\delta_0}^{\delta_u}(P_{\mathrm{m}}-P_{\mathrm{e}})\,\mathrm{d}\delta=E_{RE}(\delta_u)=0\tag{27}$$

which reveals that the EAC method can be generally expressed in the form of relative energy for a specific operating status.

4 Real-time emergency control scheme

4.1 Critical machines cluster identification

Determining generators that are at risk of going out-of-step during a given fault condition is the key step in an emergency control scheme. This process is commonly referred to as the CMC identification [19]. Various parameters such as post-fault angular separation, generator frequency, kinetic energy and ratio between acceleration power and the inertial coefficient have been employed for CMC identification in the literature [20]. In practice, under specific operational conditions, the generators in large-scale power systems might desynchronise and as a result are clustered into more than two groups according to the similarity of trajectory change. However, significant research [12, 20] has shown that at the very beginning of generators grouping, e.g. a number of cycles, the power angle trajectories are normally clustered into two groups. Especially for realistic power grids, due to the large presence of inertia as well as the resynchronisation effect, it is difficult to observe multi-clustering desynchronisation phenomenon right after fault clearance [21]. Usually, the third or more clusters of machines are gradually drawn from the initially leading group. However, during the specific interval after fault clearance, it is accepted that all the generators are considered to be contained in the two clusters.

Since the post-fault oscillations of the generators reflect the complex dynamic behaviour of the system, the CMC can be identified using the following two features: The first feature is the relative kinetic energy which is determined by the deviation from synchronous speed. The second is the variation of system absorption capacity for the relative kinetic energy due to the change of network topology after the fault. The parameters K_{RE} and P_{RE}, defined in Section 2, show the oscillation pattern of the pair-wise generators. Assuming generators buses as vertices and pair-wise generators relative energy $K_{\mathrm{RE}}=f(\cdot)$ and $P_{\mathrm{RE}}=g(\cdot)$ as an edge, the undirected edge weighted graph of N generators system is presented in Fig. 4. As shown in the graph, the clustering partition algorithm alongside with the graph theory can be used to identify the pattern of the generators separation after fault clearance.

To guarantee the speed and accuracy of CMC identification, when considering the different fault clearing times between the near and far end of each line, a new trajectory vector is yielded by the pair-wise generators relative energy within 40 ms after fault clearance. Subsequently, the aforementioned K_{RE} and P_{RE} indices are further utilised in an unsupervised spectral clustering (SC) [22] for CMC and NMC identification. This process begins by forming a graphical representation of the generator interactions. From the graph, a weighted adjacency matrix can be constructed and its Laplacian matrix is further used in the separation trajectory pattern recognition. Finally, utilising the trajectory pattern, it is straightforward to determine which generators are tending towards instability, and separating from the remaining generators by using a simple clustering analysis method. This allows us to define the CMC and NMC, accomplishing the necessary component of the stability analysis method. Specifically, the CMC identification procedure is applied by the following steps.

Step 1: Construct the weighted adjacency matrix $\boldsymbol{A}$, where each entry of $\boldsymbol{A}$ is set as the corresponding pair-wise relative energy value Ψ_{ij}

$$A_{ij}=\psi_{ij}=|f_{ij}|+|g_{ij}|=\psi_{ji}=A_{ji}\tag{28}$$

Step 2: Form the diagonal degree matrix $\boldsymbol{D}$ of the graph as

$$D_{ii}=\sum_{j=1}^{N}\psi_{ij}\tag{29}$$

where all off-diagonal elements of $\boldsymbol{D}$ are equal to zero.

Step 3: Calculate the Laplacian matrix of the gragh as

$$\boldsymbol{L}=\boldsymbol{D}-\boldsymbol{A}\tag{30}$$

and compute the spectrum via eigendecomposition as

$$\boldsymbol{L} = \mathbf{X}\Lambda\mathbf{X}^{-1} \tag{31}$$

which has a zero eigenvalue and $N-1$ non-zero eigenvalues with their corresponding eigenvectors.

Step 4: Sort the $N-1$ non-zero eigenvalues from greatest to least as $\lambda_1 \geq \lambda_2 \geq \ldots \geq \lambda_{N-1}$, and a similar reordering is applied to the corresponding eigenvectors.

Step 5: Form the separation trajectory by utilising the eigenvector corresponding to the $N-1$ non-zero eigenvalues as

$$\boldsymbol{T} = \lambda_1 x_1 + \lambda_2 x_2 + \cdots + \lambda_{N-1} x_{N-1} \tag{32}$$

which projects the scaled eigenvectors corresponding to the $N-1$ non-zero eigenvalues onto a single trajectory vector $\boldsymbol{T}$.

Step 6: Use a simple clustering analysis method (e.g. *K*-means) to identify the CMC and NMC within 40 ms after fault clearance from the trajectory pattern $\boldsymbol{T}$.

4.2 Emergency control implementation

When the power system is subjected to a severe disturbance, e.g. a three-phase short circuit, the selective tripping of generating units for severe transmission system contingencies has been used as a method of improving system stability for many years. The generation curtailment executed at an appropriate location in the system is able to reduce the power transferred through the critical transmission interfaces. Since generating units can be tripped rapidly, this is a highly effective means of adjusting disturbed power deviation and in addition ensuring the global transient stability.

According to the equivalent system energy features at the control implementation point shown in (25), the generation curtailment ΔP_{m} can be calculated as

$$\Delta P_{\mathrm{m}} = \frac{2\left(E_{\mathrm{RE}}(\delta_{\mathrm{d}}) - \int_{\delta_{\mathrm{d}}}^{\delta_{\mathrm{u}}} (P_{\mathrm{eIII}} - P_{\mathrm{m}})\,\mathrm{d}\delta\right)}{\delta_{\mathrm{u}} + \delta_{\mathrm{u}}' - 2\delta_{\mathrm{d}}} \tag{33}$$

where the angle δ_{d} and speed ω_{d} at the control action point can be measured by installed PMUs.

It is assumed that the pre-fault mechanical power is equal to the pre-fault electromagnetic power value. A curve fitting prediction model [23] utilising the PMU data from fault clearing point to the control point is therefore used to calculate the fault cleared electromagnetic power $P_{\mathrm{e\,III}}$ and post-fault unstable angle δ_{u}. Generally, the UEP of the power system is changed with a reduction of mechanical power ΔP_{m}. In this case, the awareness of UEP δ_{u}' is iteratively coupled with solving the mechanical power ΔP_{m} that needs to be curtailed. In order to rapidly estimate the amount of curtailment, the δ_{u} at the UEP without any curtailment is used to replace the power angle of the UEP with control action, namely δ_{u}'. Although the quantity of curtailment computed by using the replaced parameter δ_{u} is slightly higher than the accurately determined minimal curtailment, the latter is difficult to calculate for realistic power systems. Despite not being a theoretically global solution, this conservative result is widely acknowledged to provide adequate control performance to ensure transient stability. Considering $\delta_{\mathrm{u}}' = \delta_{\mathrm{u}}$, (33) can be rewritten as

$$\Delta P_{\mathrm{m}} = \frac{E_{\mathrm{RE}}(\delta_{\mathrm{d}}) - \int_{\delta_{\mathrm{d}}}^{\delta_{\mathrm{u}}} (P_{\mathrm{eIII}} - P_{\mathrm{m}})\,\mathrm{d}\delta}{\delta_{\mathrm{u}} - \delta_{\mathrm{d}}} \tag{34}$$

which determines the necessary generation curtailment of the post-fault unstable system.

Therefore, the imbalance of electromechanical power caused by a severe fault is determined by the trajectory-tracking-based method, rather than the complete mathematically modelled approach. The trajectory-based control scheme is also acknowledged as a highly efficient method that facilitates an online stabilisation strategy for power systems emergency control.

4.3 Generator selection for power curtailment

In addition to determining the generation power curtailment, the location of such curtailment has to be suitably selected. The previously proposed method [12] that utilises output proportion to redistribute curtailment amounts is suboptimal according to the sensitivity analysis of generation output variation. The maximum angular separation does not necessarily determine the most critical machine. Therefore, choosing heuristic ranking generation or angular separation in CMC as the selection criteria for the generation curtailment location cannot guarantee the most effective form of system instability prevention.

Referring to the pair-wise relative energy, the relative energy degree of CMC generators at control implementation point can be written as

$$D_i(t_{\mathrm{d}}) = \sum_{i \in G_{\mathrm{cc}},\, j \notin G_{\mathrm{cc}}} \left(\left|K_{REi-j}(t_{\mathrm{d}})\right| + \left|P_{REi-j}(t_{\mathrm{d}})\right|\right) \tag{35}$$

which is a measure of the relative oscillatory behaviour between the generator i among CMC and the other NMC generators. This measure consists of the two absolute values of the relative energy. One is the relative kinetic energy that represents the mechanical kinetic energy oscillation between the candidate of the most critical generator and the other NMC generators. The higher value of the $K_{\mathrm{RE}i-j}$ indicates more mechanically accelerated power. The other is the relative potential energy which indicates the network potential energy oscillation between generators. This means that generator i has the maximum potential energy with the biggest numerical value $P_{\mathrm{RE}i-j}$. So the most leading generator causing instability should be the one which has the maximum relative kinetic energy showing the biggest acceleration among the CMC and has the maximum relative potential energy representing the greatest network potential energy oscillation. The most appropriate curtailment objective for stabilising the system would be the generator which has the maximum relative energy, that is, makes a greater contribution to the system stability among the CMC in the post-fault state. Thus, the relative energy degree ranking index can be employed as an indicator to select the generation curtailment location. The higher value of this index for a generator gives it a higher priority for curtailment control implementation.

4.4 Flow chart

It is assumed that PMUs have been installed at the generators buses and a reliable transmission of the measurement data and control commands are ensured by a WAMS infrastructure. The flow chart of the proposed real-time transient stability analysis and emergency control emergency control scheme is shown in Fig. 5.

In the proposed approach to real-time transient stability analysis and emergency control scheme, the first step is utilising the pair-wise relative energy to identify the CMC and the NMC accurately during the specific interval after fault clearance. The second step is the derivation of the equivalent SIME based on the reliable clustering result and analysing the energy feature of post-fault power system to compute the reasonable generation curtailment for this equivalent SIME system. Finally, the pair-wise relative energy within the CMC is used to determine the most appropriate control location.

Additionally, as a result of the curve fitting prediction model after fault clearance, the CMC generators may change and the admittance matrix of the equivalent system may alter after the emergency control. Thus, a single open-loop control may not be able to secure the system after the first generation curtailment. An accurate emergency control scheme is close-loop feedback consisting of real-time measurements and rapid implementation. This entire process has to be monitored in a timely manner in order to ensure power system stability. If the initial emergency control fails to synchronise the system, then a further process will be launched for the next round of control until the system is stabilised.

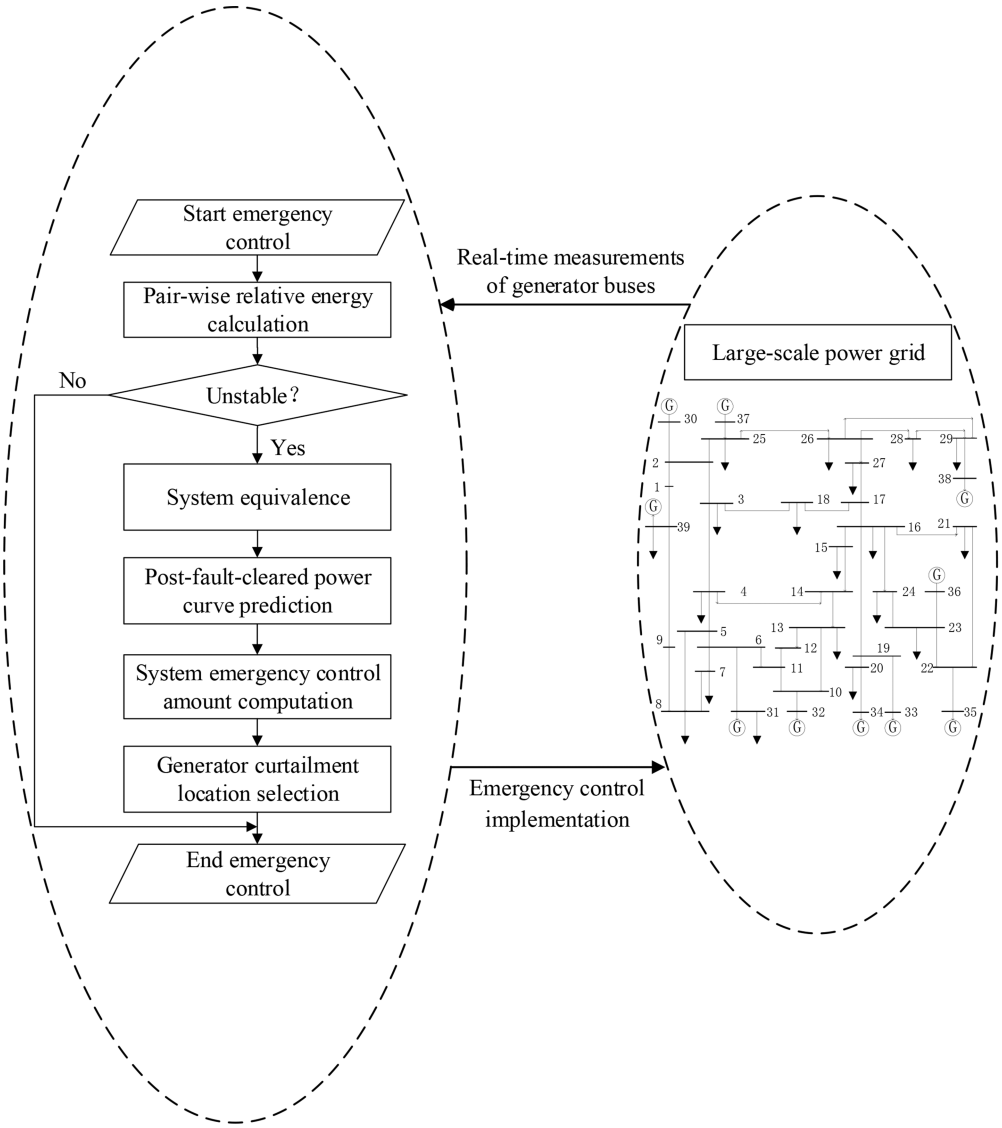

Fig. 5 *Flow chart of real-time transient stability analysis and emergency control scheme*

5 Case analysis

5.1 Transient stability analysis

In this section, the widely used New England 10 machines 39-bus dynamic system [24] with typical governors and exciters configuration has been selected to validate the effectiveness of the proposed approach. The proposed method is tested for various fault conditions as listed in Table 1. The fault list is carefully selected to severely reduce the stability of the system. The simulation platform (Power System Toolbox 3.0) is used to simulate sampling data collected from PMUs at each generator bus.

An example of generator separation for the test system is shown for fault 19 in Fig. 6*a*. If we use the engineering criterion that any two generators angle difference is >360° [25] as an indicator, the algorithm takes 1.71 s after fault clearance to detect the system transient instability.

To demonstrate the proposed method, the post-fault pair-wise relative energy trajectories for the test system are shown in Figs. 6*b* and *c*. The adjacency matrix is yielded by the pair-wise generators relative energy within 40 ms after fault clearance and further utilised in SC algorithm to identify the generator separation, which are shown in Table 2. The proposed method takes only 40 ms for instability detection and CMC identification and compares favourably with practical experience. That means, there is a suitable time interval before occurrence of the eventual instability, which can enable advanced stability control via the appropriate emergency intervention.

To benchmark the performance and speed of the proposed CMC identification method for transient stability analysis, it is compared against the use of SIME for the set of critical generators. The critical clearing time (CCT) determined via extended EAC [20] method is referred to as CCT^1, while the CCT using the proposed pair-wise relative energy method will be referred to as CCT^2 in the remainder of this section. The stability estimation for the given fault list is shown in Table 3. An obvious result from Fig. 7 shows that the pair-wise relative energy trajectories indicate which generators have higher probability of separation as system oscillations progress, which corresponds to the known critical generator as determined from time-domain simulation results. At this stage it is important to note that utilising the proposed method to identify G_9 as the critical generator yields an accurate estimate of CCT in the immediate post-fault state. In general, using the proposed approach to identify the CMC in the post-fault period evaluates the stability more accurately.

According to the CMC identification result, a curve fitting prediction model, least square fit, that utilises the PMU data from the fault clearing point to the emergency control point is used to calculate the fault cleared electromagnetic power for fault 19. The comparison of power–angle curve between simulation and fitting prediction results is shown in Fig. 7*a*. Only minor differences can be found between the predicted post-fault unstable angle $\delta_u = 127.57°$ and simulated post-control unstable angle $\delta_u' = 125.26°$. Considering the delay in receiving the measurements and the calculation latency, the emergency control strategy started by using

Table 1 *Fault list for 39-bus system*

Fault number	Fault bus and/or generator	Line cleared
F1	bus 30/gen. 1	—
F2	bus 31/gen. 2	—
F3	bus 32/gen. 3	—
F4	bus 33/gen. 4	—
F5	bus 34/gen. 5	—
F6	bus 35/gen. 6	—
F7	bus 36/gen. 7	—
F8	bus 37/gen. 8	—
F9	bus 38/gen. 9	—
F10	bus 39/gen. 10	—
F11	bus 2	line 2-3
F12	bus 4	line 4-14
F13	bus 5	line 5-8
F14	bus 6	line 6-11
F15	bus 14	line 14-15
F16	bus 16	line 16-17
F17	bus 21	line 21-16
F18	bus 23	line 23-24
F19	bus 26	line 26-28
F20	bus 27	line 27-17

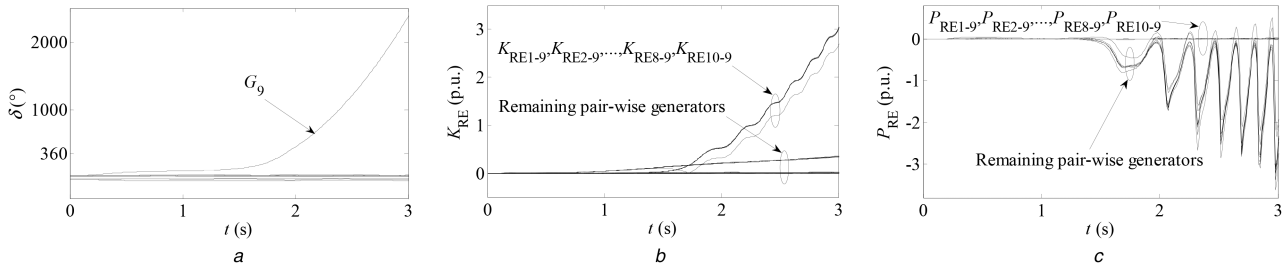

Fig. 6 *Simulation trajectories of fault 19*
(a) Rotor angle trajectories, ***(b)*** Relative kinetic energy, ***(c)*** Relative potential energy

Table 2 *SC result for CMC of fault 19*

Clustering group number	Generators
1	G_9
2	G_1, G_2, G_3, G_4, G_5, G_6, G_7, G_8, G_{10}

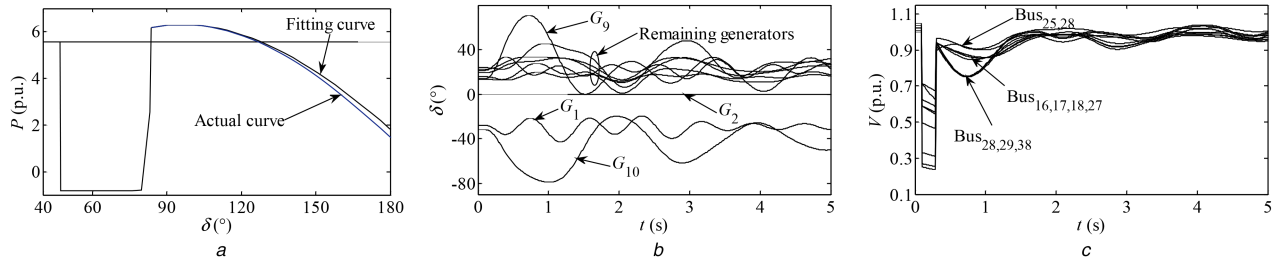

Fig. 7 *Simulation trajectories after emergency control*
(a) Power–angle prediction curve, ***(b)*** Rotor angle trajectories, ***(c)*** Bus voltage amplitude

the real-time measured values of $\delta_d = 97.43°$, $\omega_d = 1.019$ p.u. at time 160 ms after fault clearance. The required emergency power curtailment $\Delta P_m = 186.3$ MW is evaluated using the above parameters substituted into the generation curtailment calculation equation (34).

If generator G_9 is composed of four same generator units and the maximum generation curtailment is 80% of the total capacity, which is 830 MW, therefore one generator unit with 207.5 MW is selected for the generator shedding for the emergency control to stabilise the system shown in Figs. 7*b* and *c*.

5.2 Real-time emergency control implementation

A 16 machines 68-bus system has been used for the real-time emergency control study, the detailed system description of which is available in [26]. This is a reduced-order equivalent network of the interconnected New England test system and New York power system. As an example, a fault was applied at bus 16 followed by opening circuit breaker of line 16-17 with a clearing time of 300 ms. The rotor angle trajectories are shown in Fig. 8*a* for this scenario, using the same parameters as explained in the previous example. A typical multi-machine unstable mode is shown in Fig. 10 with nine generators accelerating faster than the others.

Table 3 *Fault list for 39-bus system*

Fault number	CCT[1], ms	Error of CCT[1], %	CCT[2], ms	Error of CCT[2], %	Actual CCT, ms
F1	611	41.44	472	9.26	432
F2	1241	45.83	925	8.70	851
F3	514	61.13	427	33.86	319
F4	259	54.17	180	7.14	168
F5	375	76.89	249	17.45	212
F6	461	343.27	198	90.38	104
F7	334	33.60	334	33.60	250
F8	684	93.77	446	26.35	353
F9	223	63.97	223	63.97	136
F10	542	−1.09	542	−1.09	548
F11	190	−2.56	190	−2.56	195
F12	255	21.43	220	4.76	210
F13	316	17.91	316	17.91	268
F14	265	39.47	217	14.21	190
F15	389	42.49	300	9.89	273
F16	170	6.25	170	6.25	160
F17	335	106.79	320	97.53	162
F18	240	54.84	185	19.35	155
F19	155	46.23	125	17.92	106
F20	258	17.27	258	17.27	220

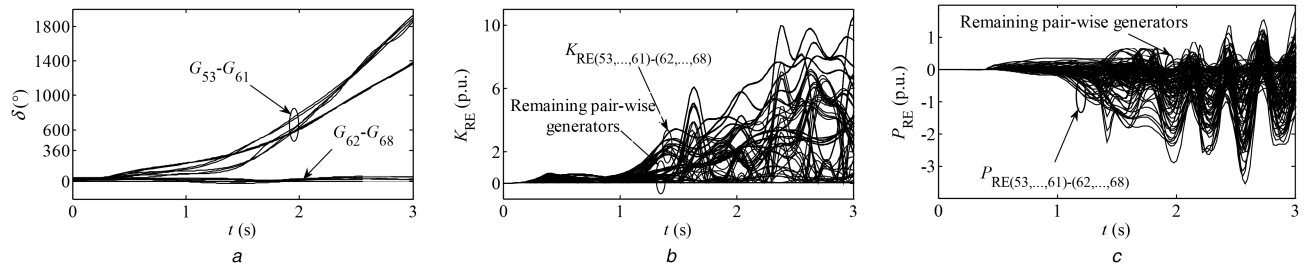

Fig. 8 *Simulation trajectories for 300 ms fault at bus 16, with a clearing of line 16-17*
(a) Rotor angle trajectories, ***(b)*** Relative kinetic energy, ***(c)*** Relative potential energy

Table 4 *SC result for CMC*

Clustering group number	Generators
1	G_{53}, G_{54}, G_{55}, G_{56}, G_{57}, G_{58}, G_{59}, G_{60}, G_{61}
2	G_{62}, G_{63}, G_{64}, G_{65}, G_{66}, G_{67}, G_{68}

System instability is identified at $t = 1.06$ s after fault clearance using the engineering criterion.

Similarly, the proposed RKES and RPES indices were calculated for the above scenario. The adjacency matrix was yielded by the pair-wise relative energy calculation within 40 ms after fault clearance and was further utilised in SC algorithm to identify the separating generator cluster. The result is shown in Table 4. The pair-wise relative energy oscillation trajectories are shown in Figs. 8*b* and *c* for this scenario.

According to CMC identification result in Table 4, it is reasonable to select G_{53}–G_{61} as CMC_S and G_{62}–G_{68} as NMC_A. The post-fault unstable angle $\delta_u = 192.31°$ is calculated using curve fitting based prediction of the equivalent electromagnetic power. The required emergency power curtailment ΔP_m is 251 MW. This parameter is evaluated using the measured values of $\delta_d = 47.24°$ and $\omega_d = 1.012$p.u., substituting them into curtailment calculation equation (34). A comparison of the proposed criterion (35) with a number of previously recommended criteria is illustrated in Table 5.

According to the compared results of different emergency control criteria shown in Table 5, the generators have dissimilar ranking places in the most critical machines selection. For example, G_{59} ranks in the first place with the largest rotor angle δ, the fastest rotor speed ω and the maximum kinetic energy V_{Kd} which indicates that G_{59} may have the most sensitivity at the emergency control point. However, G_{61} shows a potential possibility which is the most critical generator with the largest ratio between power acceleration and inertia coefficient. The remaining generators may be considered as the non-critical machines by using the conventional criteria.

Regarding the calculated generator ranking for different emergency control criteria shown in Table 5, five locations are suggested for executing generation curtailment based on the different recommended selection principle. The determined generators and their curtailment generation are shown in Table 6. The percentage shown in parenthesis represents the generation curtailment percentage of installed capacity. The rotor angle trajectories of post-control scheme are presented in Fig. 9. The simulation results show that the curtailment even up to 255 MW cannot prevent system instability using the classical criteria. Conversely, the proposed approach can stabilise the system only by emergently reducing 251 MW mechanical power.

To illustrate the effectiveness of the proposed control criterion D, a comparison of valid generation curtailment are shown in Table 7. The generator G_{58} is selected as the first recommended control object because of its highest value of relative energy degree. The simulation results prove that the proposed control criterion can stabilise the system with the minimum generation curtailment that shows its superior performance by choosing more

Table 5 *Comparison of different emergency control criteria in CMC (bold indicates recommended control generators)*

Generator	δ, deg	Rank	ω, p.u.	Rank	V_{Kd}, p.u.	Rank	P_{acc}/M, p.u.	Rank	D, p.u.	Rank
G_{53}	64.02	8	1.0036	9	0.0141	9	0.0017	6	2.68	7
G_{54}	62.83	9	1.0094	8	0.1365	7	0.0011	8	2.64	9
G_{55}	74.18	6	1.0100	7	0.1848	6	0.0017	6	2.84	6
G_{56}	105.38	3	1.0183	3	0.4358	4	0.0029	2	4.95	4
G_{57}	88.65	5	1.0173	4	0.4503	3	0.0009	9	5.00	3
G_{58}	106.57	2	1.0191	2	0.4973	2	0.0024	3	6.61	1
G_{59}	107.11	1	1.0192	1	0.5655	1	0.0021	5	5.66	2
G_{60}	70.60	7	1.0102	6	0.1292	8	0.0024	3	2.68	7
G_{61}	90.62	4	1.0127	5	0.2056	5	0.0033	1	3.02	5

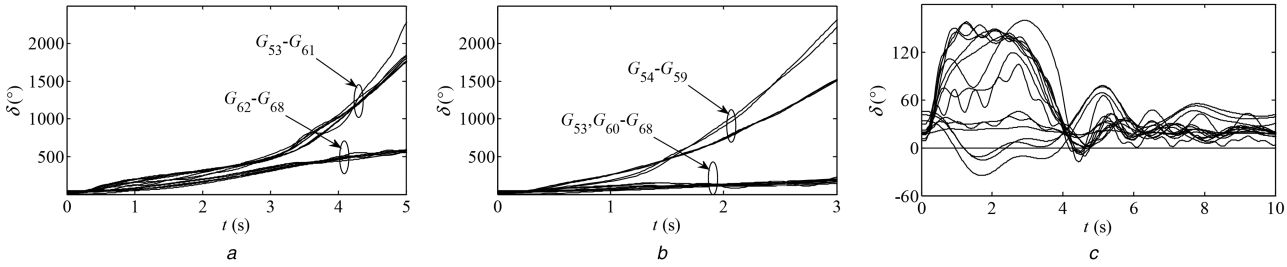

Fig. 9 *Rotor angle trajectories with different generation curtailment selections*
(a) Rotor angle trajectories with generation curtailment on G_{59}, ***(b)*** Rotor angle trajectories with generation curtailment on G_{61}, ***(c)*** Rotor angle trajectories with generation curtailment on G_{58}

Table 6 *Comparison of emergency control criteria and effects*

Control criteria	Selected generator	Control capacity, MW	Stability
δ	G_{59}	255(45.54%)	unstable
ω	G_{59}	255(45.54%)	unstable
V_{Kd}	G_{59}	255(45.54%)	unstable
P_{acc}/M	G_{61}	255(31.88%)	unstable
D	G_{58}	251(35.86%)	stable

Table 7 *Comparison of generation curtailment and effects for the relative energy degree index D*

Rank	Generator	D, p.u.	Generation capacity, MW	Minimum curtailment, MW	Curtailment percentage, %	Stability
1	G_{58}	6.61	700	251	35.86%	stable
2	G_{59}	5.66	560	257	45.89%	stable
3	G_{57}	5.00	505	334	66.14%	stable
4	G_{56}	4.95	632	340	53.80%	stable
5	G_{61}	3.02	800	800	100%	unstable
6	G_{55}	2.84	650	650	100%	unstable
7	G_{53}	2.68	250	250	100%	unstable
7	G_{60}	2.68	540	540	100%	unstable
9	G_{54}	2.64	545	545	100%	unstable

appropriate locations. In this case, theoretically, the proposed technique is able to meet the requirements of real-time measurement, online strategy determination and prompt emergency control.

5.3 Impact of PMU measurement noise and interruption

Even in situations where the dynamic power system model contains sufficiently accurate information, many proposed methods for stability estimation require the timely delivery of accurate system measurements. The objective of this section is to assess the impacts of measurement quality on the stability analysis of PMUs deployed power systems based on the presented relative energy approach.

In these tests, New England 10 machines 39-bus dynamic system is used considering two separate fault conditions. The first fault condition (fault 1) is a 100 ms fault occurring at the bus 33 generator G_4. The second fault condition (fault 2) is a 100 ms fault at non-generator bus 14. For both test cases, it is assumed that PMU is deployed at each generator-connected bus for gathering real-time phasor information, providing the continuous measured data to support the presented pair-wise relative energy stability analysis.

For this analysis, it is important to note that the PMU source of poor data and the method addressing the data quality will both have a significant impact on the estimate error of transient stability. In order to check robustness of the proposed algorithm under noisy measurements, simulations have been completed with Gaussian noise. The signal-to-noise ratio (SNR) is tested from 100 to 10 dB for the overall ten PMUs. The simulation results are shown in Fig. 10.

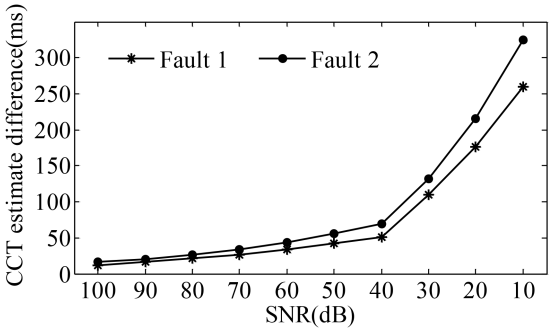

Fig. 10 *Impact of PMU measurement noise data on the CCT estimates*

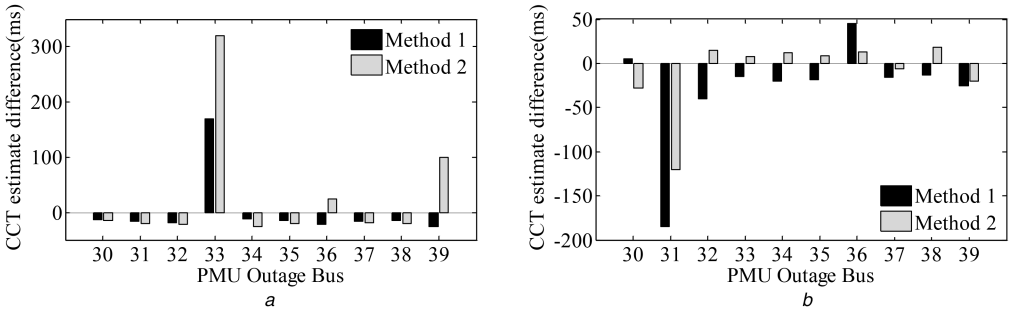

Fig. 11 *Impact of missing or corrupted PMU data on the CCT estimates*
(a) For a 100 ms fault at the bus for generator G_4, ***(b)*** For a 100 ms fault at bus 14, with a clearing of line 14-15

Simulation results show that the proposed method works well even within the measurement noise produced by PMU devices. The algorithm can restrict the CCT estimate difference to <60 ms even with SNR 40. For commercially available PMUs, SNR is normally higher than 100 (total vector error is <1%). It means the magnitude of the noise is always <1% of the measured signal magnitude. So the proposed method can tolerate 2.5% noise, which is more than the maximum noise in actual PMU measurements.

Moreover, for both fault test cases, a subset of hypothetical worst case conditions is considered, where each of the ten PMUs is individually considered to have lost data transmission capability. Subsequently, the data quality issues are addressed via two possible methods: method 1, where the missing PMU data is replaced with the static quantities obtained from the most recently available steady-state measurement, and method 2, where the generator for which the PMU data is missing is removed from the transient model entirely. The simulation results are displayed in Fig. 11.

As seen in Fig. 11*a*, though each of the ten test cases represents an equivalent loss in overall data quality, the impacts on the CCT estimate do not vary linearly with respect to the geographical source of the loss of PMU data. As might be intuitively expected, the loss of the PMU data stream nearest to the fault occurrence leads to the most significant errors in the estimate. Fig. 11*b* displays a similar pattern of non-linear data quality impacts, showing that the location of PMU loss is a critical factor in obtaining accurate CCT estimates. In this case, the loss of the PMU located closest to the generator which would first go out-of-step yields the greatest estimation errors. It is also important to note that the sign of the estimation error may also vary, which may cause further difficulty in these cases since it would be difficult to attempt to discern if the erroneous CCT estimate was an over-estimate or an underestimate.

6 Conclusion

In this paper, it has been shown that the proposed relative energy function of pair-wise generators can provide valuable insights with regard to transient stability analysis and emergency control. The derivation of the method showed that the pair-wise relative energy utilised in this study provides an equivalent measure of post-fault system transient energy to that of the original TEF. The proposed formulation of the pair-wise generator relative energy has eliminated any dependence on network properties, allowing the indices to be derived directly from generator bus measurements obtained from installed PMUs. Consequently, the method can be readily applied to accurately identify the CMC during post-fault swings without the need for any information about the location of the fault or network parameters. According to the CMC identification results, using the proposed approach to identify the CMC in the post-fault period leads to more accurate stability estimates when compared with the exiting approaches. Additionally, the quantity of generation curtailment and the new emergency control criterion were proposed in order to stabilise the system within a comparatively short interval after fault clearance. The proposed method outperforms the previously studied stability control criteria in terms of generation curtailment calculation and appropriate location selection.

7 References

[1] Begovic, M.: '*Electrical transmission systems and smart grid: selected entries from the encyclopedia of sustainability science and technology*' (Springer, New York, 2012)

[2] Andersson, G., Donalek, P., Farmer, R.*, et al.*: 'Causes of the 2003 major grid blackouts in North America and Europe, and recommended means to improve system dynamic performance', *IEEE Trans. Power Syst.*, 2005, **4**, pp. 1922–1928

[3] Hines, P., Balasubramaniam, K., Sanchez, E.: 'Cascading failures in power grids', *IEEE Potentials*, 2009, **5**, pp. 24–30

[4] Zarco, P., Gomez, A. E.: 'Power system parameter estimation: a survey', *IEEE Trans. Power Syst.*, 2000, **1**, pp. 216–222

[5] Zhang, Y., Wehenkel, L., Rousseaux, P.*, et al.*: 'SIME: a hybrid approach to fast transient stability assessment and contingency selection', *Int. J. Electr. Power Energy Syst.*, 1997, **3**, pp. 195–208

[6] Zarate-Minano, R., Van Cutsem, T., Milano, F.*, et al.*: 'Securing transient stability using time-domain simulations within an optimal power flow,' *IEEE Trans. Power Syst.*, 2010, **1**, pp. 243–253

[7] Padiyar, K., Krishna, S.: 'Online detection of loss of synchronism using energy function criterion,' *IEEE Trans. Power Deliv.*, 2006, **1**, pp. 46–55

[8] Krishna, S., Padiyar, K. R.: 'On-line dynamic security assessment: determination of critical transmission lines', *Electr. Power Compon. Syst.*, 2009, **2**, pp. 152–165

[9] Chow, J., Chakrabortty, A., Arcak, M.*, et al.*: 'Synchronized phasor data based energy function analysis of dominant power transfer paths in large power systems', *IEEE Trans. Power Syst.*, 2007, **2**, pp. 727–734

[10] Cai, G. W., Chan, K. W., Yuan, W. P.*, et al.*: 'Identification of the vulnerable transmission segment and cluster of critical machines using line transient potential energy', *Int. J. Electr. Power Energy Syst.*, 2007, **3**, pp. 199–207

[11] Ota, H., Kitayama, Y., Ito, H.*, et al.*: 'Development of transient stability control system (TSC system) based on on-line stability calculation', *IEEE Trans. Power Syst.*, 1996, **3**, pp. 1463–1472

[12] Pavella, M., Ernst, D., Ruiz-Vega, D.: '*Transient stability of power systems: a unified approach to assessment and control*' (Sringer US, 2000)

[13] Ruiz-Vega, D., Pavella, M.: 'A comprehensive approach to transient stability control. I. Near optimal preventive control', *IEEE Trans. Power Syst.*, 2003, **4**, pp. 1446–1453
[14] Ruiz-Vega, D., Pavella, M.: 'A comprehensive approach to transient stability control. II. Open loop emergency control', *IEEE Trans. Power Syst.*, 2003, **4**, pp. 1454–1460
[15] Saunders, C. S., Alamuti, M. M., Taylor, G. A., *et al.*: 'Utilizing generator pair-wise potential energy functions for critical generator estimation'. IEEE PES General Meeting 2015, Denver, USA, July 2015
[16] Anderson, P., Fouad, A.: '*Power system control and stability*' (IEEE Press, 2003)
[17] Fang, D. Z., Chung, T. S., Zhang, Y., *et al.*: 'Transient stability limit conditions analysis using a corrected transient energy function approach', *IEEE Trans. Power Syst.*, 2000, **2**, pp. 804–810
[18] Fang, D. Z., Jing, L., Chung, T. S.: 'Corrected transient energy function-based strategy for stability probability assessment of power systems', *IET Gener. Transm. Distrib.*, 2008, **3**, pp. 424–432
[19] Weckesser, T., Jóhannsson, H., Østergaard, J.: 'Critical machine cluster identification using the equal area criterion'. 2015 IEEE Power & Energy Society General Meeting, Denver, USA, July 2015, pp. 1–5
[20] Xue, Y., Pavella, M. R.: 'Extended equal-area criterion: an analytical ultra-fast method for transient stability assessment and preventive control of power systems', *Int. J. Electr. Power Energy Syst.*, 1989, **2**, pp. 131–149
[21] Liu, Y., Liu, Y., Liu, J., *et al.*: 'High-performance predictor for critical unstable generators based on scalable parallelized neural networks', *J. Mod. Power Syst. Clean Energy*, 2016, **3**, pp. 414–426
[22] Ding, L., Gonzalez-Longatt, F., Wall, P., *et al.*: 'Two-step spectral clustering controlled islanding algorithm', *IEEE Trans. Power Syst.*, 2013, **1**, pp. 75–84
[23] Xue, Y., Cutsem, T. V., Pavella, M. R.: 'A simple direct method for fast transient stability assessment of large power systems,' *IEEE Trans. Power Syst.*, 1988, **2**, pp. 400–412.
[24] Pai, M. A.: '*Energy function analysis for power system stability*' (Springer, 1989)
[25] Gomez, F., Rajapakse, A., Annakkage, U., *et al.*: 'Support vector machine-based algorithm for post-fault transient stability status prediction using synchronized measurements', *IEEE Trans. Power Syst.*, 2011, **3**, pp. 1474–1483
[26] G. E. Company, U. S. D. of Energy Office of Energy Systems Research: 'Singular perturbations, coherency and aggregation of dynamic systems', U.S. Department of Energy, 1983